Title:
Analytical friction model for sliding bodies with coupled longitudinal and transverse vibration

Authors:
Priyang Udaykant Jadav [a,c] *(Corresponding author)*
Priyang.Jadav@rotork.com

Ramin Amali [a]
Ramin2.Amali@uwe.ac.uk

Oluwamayokun Adetoro [b]
Mayo.Adetoro@brunel.ac.uk

[a] Department of Engineering Design and Mathematics, University of the West of England, Bristol, BS16 1QY, United Kingdom
[b] Department of Mechanical and Aerospace Engineering, Brunel University London, Uxbridge, UB8 3PH, United Kingdom
[c] Rotork Controls Ltd, Bath, BA1 3JQ, United Kingdom

ABSTRACT

An analytical friction model is developed to calculate the drive force required to slide a body over a surface that is subjected to coupled longitudinal and transverse vibration. Previously, this computation was only possible under either longitudinal or transverse vibration using a separate analytical model for each mode. This paper presents a development of recent research in which it is possible to use a single analytical model, developed in Matlab®/Simulink®, to compute the friction force and drive force during longitudinal, transverse and coupled longitudinal-transverse vibration. The new model is also evaluated numerically by use of a specially developed friction subroutine which can be integrated into any Abaqus® dry contact simulation. Results agree very well with those in previously published literature.

Keywords: Friction, Vibration, Modelling, Analytical

---

1. Introduction

In mechanical systems that involve predominantly dry sliding contacts the efficiency of the system can be significantly improved by reducing the friction force between the rubbing surfaces. This is usually achieved by improving the surface quality of the contacting pair, utilising conventional lubricants [1-3] or those enhanced with nano-particles [4-6], or by applying surface coatings [7,8]. A less typical method of friction reduction and one that has been the subject of theoretical analyses for several decades is the phenomenon of reduced friction force of surfaces when subjected to vibration. Frictional forces may cause undesired vibrations in a system as a result of stick-slip motion at the contact, conversely, many studies [9-25] have shown that imposed vibration can significantly reduce the friction force between two contacting surfaces. In such studies the vibration is applied to the contact by exciting one of the contacting bodies in the normal, longitudinal or transverse direction.

Considerable research has been devoted to exploiting this phenomenon in various manufacturing processes. Jimma et al. [26] found that vibration applied to the deep drawing process enables deeper cups to be formed whilst avoiding cracks in steel drawn parts, Siegert and Ulmer [27] showed that it is possible to further reduce the friction force by having the drawing dies vibrate parallel to the drawing direction at frequencies ranging 20-22 kHz. Egashira et al. [28] utilised vibration whilst drilling micro holes in glass to reduce the cutting force and extend tool life. In the food industry, vibrating blades are used to reduce friction when cutting through foods [29]. Screws can also be tightened with considerably less torque through an instantaneous reduction in the friction force supplied by vibration.

The first work investigating the influence of vibration on friction dates back to a 1952 study by Baker et al. [9] in which they determined that the coefficient of static friction under the influence of imposed normal vibration can been minimised to almost zero. Experiments by Fridman and Levesque [10] and also by Godfrey [11] showed that pulling a block of mass over a plate vibrating perpendicular to the contact, with increasing vibration amplitude, reduces the static friction coefficient by almost 100%. One of the first attempts to explain friction force reduction due to normal vibration was made by Lenkiewicz [12]; vibrations forced perpendicularly or at an angle to the friction surface generally cause changes in the value of the real contact area, and consequently changes in the value of the friction force. This is in agreement with Hess and Soom [13] who concluded that a temporary debonding of the contact surfaces leads to a reduction in the mean area of contact and a corresponding reduction in friction. In this century, normal vibration applied in custom built pin-on-disk tribometers have shown a decrease in friction coefficient with increasing vibration frequency and amplitude, between both metallic [14] and non-metallic surfaces [15].

In the case of longitudinal vibration conjecture, until recently, has been that the reduction of average friction force occurs as a result of cyclic instantaneous changes in the direction of the friction force vector, caused by changes in the sign of relative velocity when the amplitude of vibration velocity is greater than the velocity of sliding motion [16-22]. Gutowski and Leus [23] have shown that this commonly accepted view is erroneous. Reduction of average friction force may also take place without the change in sign of the friction force vector. One of the reasons behind the antiquated view is that in

friction force estimations, the simplified static friction models based on the Coulomb model of friction are assumed. In these models the deformation in the contact zone of two surfaces moving in relation to one another is not taken into consideration. This creates significant difficulties in the conduct of simulational analyses due to their insufficient consistency with experimental results. Gutowski and Leus [23] have shown that significantly better results can be achieved by conducting the analyses using dynamic friction models, such as the Dahl or Dupont model in which the real elasto-plastic characteristics of the contact are considered. Analyses carried out with the use of Dahl friction model yield very good agreement between computations and experimental results.

During transverse vibration a variable vector of relative velocity of sliding causes oscillations of the friction force vector around the sliding direction, resulting in a sub-division of this force into two components, one parallel (F_x) and one perpendicular (F_y) to the direction of motion, see Fig. 3c. Consequently, only the parallel component of friction force acts in the direction of motion, resulting in the reduction of driving force F_d required in this direction. Investigations [18-22] based on this mechanism have also shown a large discrepancy between analytical and experimental results since the analytical models are based on the Coulomb friction model. Gutowski and Leus [24] again demonstrated that a much better agreement can be achieved by utilising an analytical model which considers dynamic friction together with dynamic equations of motion, whilst also including terms to describe the compliance of the mechanical drive system.

This paper focuses on the latter two modes of vibration that are tangential to the plane of contact. Tsai and Tseng [25] assumed that tangential vibrations are imposed directly onto the sliding body and analysed the effect on friction force reduction. They used the Dahl friction model [30,31] on a single lumped elastic asperity to investigate the reduction phenomenon. Gutowski and Leus [23,24] on the other hand, applied vibration to the base and assumed that this vibration is transferred to the sliding body. They developed an analytical model for longitudinal vibration and a separate model for transverse vibration, however, a model for coupled longitudinal-transverse vibration does not exist in literature. This paper proposes a new model, based on the approach of Gutowski and Leus [23,24], to describe the changes in friction force and drive force for sliding surfaces subjected to coupled vibration. The previous models [23,24] are used as basis for validating the new model.

There are four objectives of the work presented in this paper; (i) derivation of a mathematical model that can be used to determine quantitative changes in the friction force occurring at the contact between the sliding body and the base which is under the influence of longitudinal, transverse or coupled vibration (ii) simulation of the new model both analytically in Matlab®/Simulink® and numerically in Abaqus® (iii) validation of the new model by comparison of results with analogous ones in previous publications (iv) analysis of how the drive force F_d is influenced by different modes of imposed coupled vibration.

2. Model formulation

Dahl [30] discovered that when an external drive force is applied on a static body that is in contact with another, an intermediate motion of one surface over the other occurs before the bodies enter macroscopic relative motion. This intermediate motion is often described as pre-sliding displacement, otherwise termed “elastic slip”, and is the result of real surfaces having asperities that interlock when two surfaces are in contact. The application of external drive force on the body initially creates an elastic deformation of the contacting asperities. As the asperities undergo increased strain, yielding occurs and the two surfaces then start to break free of each other. During this time plastic deformation of asperities takes place. Finally, asperity rupture occurs leading to formation of further surface irregularities which will continuously undergo strain and rupture as sliding takes place [30]. Thus, in Dahl’s dynamic friction model it is assumed that the friction force F is associated with the elastic deformation s of the contact (Fig. 1) measured in the direction of sliding:

$$F = k_t s \tag{1}$$

where k_t is the stiffness of the contact in the tangential direction. This is illustrated in Fig. 1 where the deformable contacting asperities of the sliding body and the base are thought of as a single lumped asperity MN.

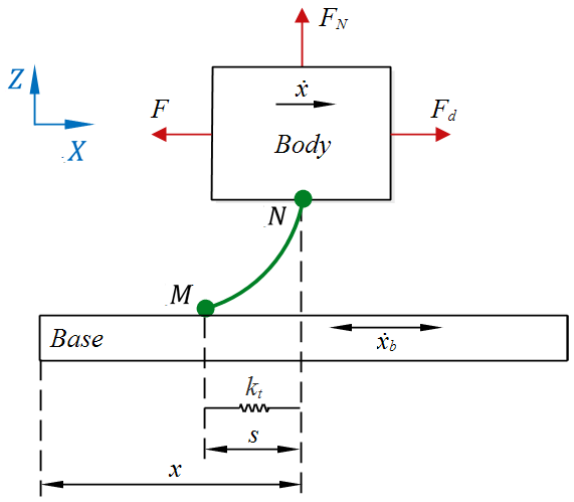

Fig. 1. Elastic strain 's' of contact zone assumed in Dahl's friction model

The force-displacement relationship is modelled by Dahl [31] with the following differential equation:

$$\frac{dF}{dx} = \begin{cases} k_t \left[1 - \frac{F}{F_C}\text{sgn}(\dot{x})\right]^i & if\ i > 0 \\ k_t & if\ i = 0 \end{cases} \tag{2}$$

where dF and dx are the incremental friction force and incremental displacement respectively, and $\dot{x}$ is the instantaneous velocity of the body in the direction of sliding. F_C is the magnitude of Coulomb friction force, given by:

$$F_C = \mu F_N \tag{3}$$

where μ is the coefficient of static friction and F_N is the normal reaction force.

The parameter i in equation (2) determines the shape of the relationship between the tangential displacement x and friction force F. $i = 0$ describes brittle material behaviour, where the friction force linearly increases with tangential displacement at a gradient k_t (Fig. 2), until the maximum friction force is reached and the surfaces break away. This maximum force is equal to the Coulomb friction force F_C. As the value of $i \to 2$ the material behaviour becomes ductile producing a non-linear response of F which is asymptotic to the value of F_C [31]. The value $i = 1$ is used for all computations in this paper.

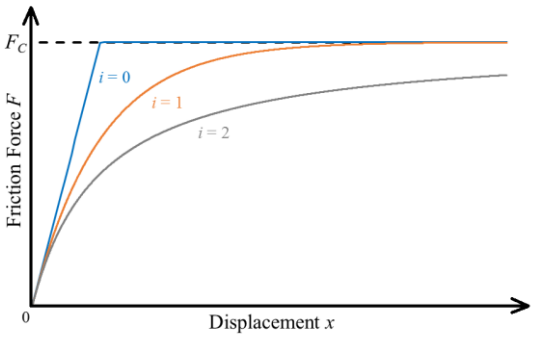

Fig. 2. The effect of parameter i on the relationship between friction force F and displacement x

By substituting (1) and (3) into (2), the relationship can be written in the form of (4), which describes the relationship between the velocity of contact deformation ds/dt and the velocity $\dot{x}$ of the sliding body.

$$\frac{ds}{dt} = \dot{x}\left[1 - \frac{k_t s}{\mu F_N}\mathrm{sgn}(\dot{x})\right]^i \tag{4}$$

The instantaneous velocity $\dot{x}$ can be thought of as the relative velocity v_r of the sliding body in relation to the base velocity $\dot{x}_b$ (Fig. 1), where:

$$v_r = \dot{x} - \dot{x}_b = \begin{cases} \dot{x} & if\ \dot{x}_b = 0, \text{i. e. stationary base} \\ v_r & if\ \dot{x}_b \neq 0, \text{i. e. vibrating base} \end{cases} \tag{5}$$

Therefore (4) can be written in a generalised form which takes into account both the non-vibrating and vibrating cases:

$$\frac{ds}{dt} = v_r\left[1 - \frac{k_t s}{\mu F_N}\mathrm{sgn}(v_r)\right]^i \tag{6}$$

Fig. 1 depicts the case of longitudinal vibration which is a one-dimensional problem; the vibration of the base acts parallel to the direction of sliding of the body therefore deformation s of elastic asperity MN occurs in one dimension. Equation (6) can be readily used in this case.

In transverse, or coupled longitudinal-transverse vibration, the problem becomes two dimensional since the deformation s no longer occurs parallel to the direction of sliding. Equation (6) therefore cannot be readily used in these cases. Gutowski and Leus [24] developed a mathematical model for computing friction force during transverse vibration. In the following work it is shown that the transverse vibration model can be extended for use with longitudinal and coupled longitudinal-transverse vibration.

Mathematical computational procedures were developed assuming the Dahl model in combination with the experimental setup described by Gutowski and Leus [23,24]. Their specially designed test rig comprises a body of known mass m moved over a base that can be vibrated by a piezoelectric element either in the longitudinal or transverse mode. Fig. 3a is a schematic representation of their setup with the assumption, for the purposes of this paper, that vibration can be applied not only in longitudinal (X) or transverse (Y) mode but can also be coupled so that longitudinal and transverse components act simultaneously and in phase. Mathematically this is equivalent to applying the vibration along an axis that is at an arbitrary angle θ (Fig. 3b) relative to the direction of sliding. Angle θ thus describes the mode of vibration. The displacement of the base during this coupled vibration can be separated into longitudinal and transverse components x_b and y_b respectively.

The movement of mass m over the base is imposed by a constant drive velocity v_d applied at point B (Fig. 3a), while sinusoidal vibration applied to the base is also transferred to the body, corresponding to an instantaneous external drive force F_d. The drive force is transferred to point A of the sliding body via the drive system of which the stiffness coefficient k_d is known and zero structural damping is assumed, hence $h_d = 0$. Endpoint N of the lumped asperity is attached to the sliding body, while the free endpoint M interfaces with the vibrating base. N' is the projection of N on the plane of sliding XY. Relative displacement of points M and N' creates the deformation s of the contact at an angle β measured in the XY plane.

In transverse vibration [24] the motion of the body sliding over the vibrating base is a superposition of two motions; the first caused by the driving force F_d, and the second by the transfer of transverse motion y_b from the base to the sliding body. When coupling longitudinal vibration to the transverse, a third motion must also be superimposed; the motion of the sliding body caused by the transfer of longitudinal motion x_b from the base. All three of these motions influence the magnitude

and direction of elastic deformation s of the contact zone. This deformation directly decides the magnitude and direction of the friction force F.

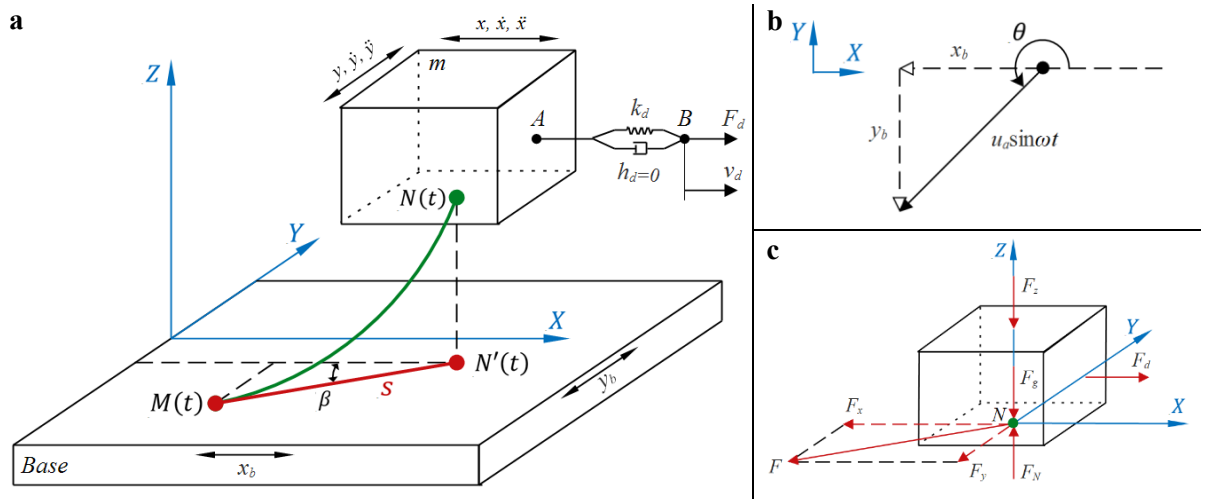

Fig. 3. (a) Contact's elastic deformation modelled as a lumped elastic asperity MN [24] (b) instantaneous displacement vector of base vibrating along an axis at angle θ, separated into components x_b and y_b (c) instantaneous forces acting on sliding body [24]

The new model is a development of previous models [23,24] and follows the formulation described by the sequence of equations henceforth using notations presented in Fig. 4. Boxed parameters indicate state variables; their value calculated in the previous increment is carried forward for use in the current increment. During a consecutive time increment Δt, points M and N' change their relative positions thus elastic deformation of the contact undergoes a change in its magnitude and direction from $s(t)$ at the beginning of the increment to $s_1(t+\Delta t)$ at the end of the increment. Coordinates of M and N', and magnitude of $s(t)$ at the start of the increment are given by:

$$M(t) = [M_x(t),\ M_y(t)] = [\boxed{M_{1x}}, \boxed{M_{1y}}] \tag{7}$$

$$N'(t) = [N'_x(t),\ N'_y(t)] = [\boxed{N'_{1x}}, \boxed{N'_{1y}}] = [\boxed{x}, \boxed{y}] \tag{8}$$

$$s(t) = \boxed{s_1} \tag{9}$$

and at the end of the increment by:

$$M(t+\Delta t) = M_1 = [M_{1x},\ M_{1y}] \tag{10}$$

$$N'(t+\Delta t) = N'_1 = [N'_{1x},\ N'_{1y}] = [x, y] \tag{11}$$

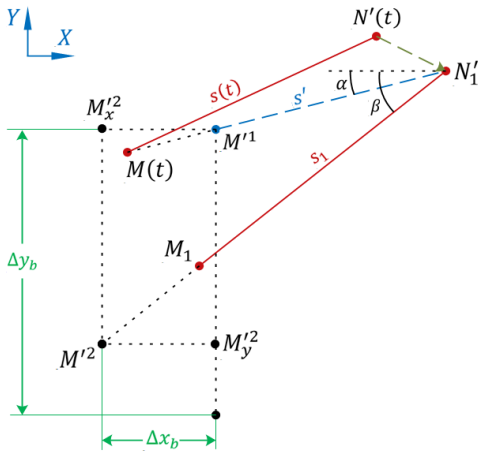

Fig. 4. Change in magnitude and direction of deformation from s to s_1 over a single time increment Δt

The position of points M and N' at any instance is a result of superposition of the motion caused by the driving force F_d, the base longitudinal vibration component x_b and transverse component y_b. At consecutive instances M and N' change their relative position, thus elastic deformation of the contact undergoes a change in its magnitude and direction from s to s_1. This change during any consecutive time increment Δt is separated into two phases. In the first phase the intermediate deformation s' is analysed as a result of motion of point N' to N_1' position. In the second phase the final deformation s_1 is analysed as a result of motion of point M'^1 to M'^2 position. The displacement from M'^1 to M'^2 is described by components $\overline{M'^1 M_x'^2}$ and $\overline{M'^1 M_y'^2}$. Since N is rigidly connected with the sliding body, its coordinates $[x, y]$ in the XY plane can be described by equations (14) and (16).

$$m\ddot{x} = F_d - F_x \tag{12}$$

$$\Delta x = \iint \frac{F_d - F_x}{m} dtdt - \boxed{\iint \frac{F_d - F_x}{m} dtdt} \tag{13}$$

$$x = \Delta x - \boxed{\Delta x_b} + \boxed{x} \tag{14}$$

where F_d, F_x and Δx_b are calculated by equations (17), (38) and (28) respectively.

$$m\ddot{y} = F_y \tag{15}$$

$$y = \iint \frac{F_y}{m} dtdt \tag{16}$$

where F_y is calculated by equation (39). F_x and F_y are components of the friction force F acting parallel to the X and Y axes respectively (Fig. 3c). Point B moves at a constant drive velocity v_d whereas the velocity of point A, being rigidly connected to the sliding body, is affected by the transfer of vibrating motion from the base to the body. Due to a continually changing position of point A relative to B, the driving force F_d does not have a constant value. It is a function of the variable elastic deformation of the mechanical drive's components. Assuming the drive system has a linear elastic characteristic, the drive force is calculated by:

$$\begin{aligned} F_d &= k_d[x_B - x_A] \\ &= k_d[v_d t - N_{1x}'] \end{aligned} \tag{17}$$

where t is time, and $N_{1x}' = x$ is the instantaneous displacement of the sliding body in the X direction, determined by equation (14).

2.1. First phase of motion

During a consecutive time interval Δt, in the first phase of motion, displacement of the sliding body occurs which moves N' to the N_1' position (Fig. 4). At the same instance, M moves along the path $\overline{MN_1'}$ to the M'^1 position. Consequently, deformation s changes to an intermediate s' with a new magnitude and direction. Instantaneous direction of this deformation is determined by angle α, whilst the change in its magnitude by an increment Δs [24]. The increment Δs can be evaluated using relationship (6), therefore, the magnitude of deformation s' after this first phase of motion is calculated by:

$$\begin{aligned} s' &= s + \Delta s \\ &= \boxed{s_1} + v_{r1}\left[1 - \frac{k_t \boxed{s_1}}{\mu F_N}\mathrm{sgn}(v_{r1})\right]^i \Delta t \end{aligned} \tag{18}$$

Relative velocity v_{r1} along the line of action of the lumped elastic asperity can be determined from the following expression:

$$v_{r1} = \frac{\overline{MN_1'} - \overline{MN'}}{\Delta t} = \frac{\overline{MN_1'} - s}{\Delta t} = \frac{\overline{MN_1'} - \boxed{s_1}}{\Delta t} \tag{19}$$

where

$$\begin{aligned} \overline{MN_1'} &= \sqrt{[N_{1x}' - M_x(t)]^2 + \left[M_y(t) - N_{1y}'\right]^2} \\ &= \sqrt{\left[x - \boxed{M_{1x}}\right]^2 + \left[\boxed{M_{1y}} - y\right]^2} \end{aligned} \tag{20}$$

Direction of v_{r1} in relation to axis X is determined by angle α (Fig. 4) where:

$$\sin\alpha = \begin{cases} \dfrac{\boxed{M_{1y}} - y}{\overline{MN_1'}} & if\ t > t_v \\ 0 & if\ t \le t_v \end{cases} \tag{21}$$

$$\cos\alpha = \begin{cases} \dfrac{x - \boxed{M_{1x}}}{\overline{MN_1'}} & if\ t > t_v \\ 1 & if\ t \le t_v \end{cases} \tag{22}$$

and t_v is the time at which vibration is switched on. The if conditions in (21) and (22) are necessary to avoid nan errors in the formulation when $\overline{MN_1'} = 0$.

2.2. Second phase of motion

Within the same time increment Δt, in the second phase of motion, in accordance with Fig. 3b, the base undergoes coupled longitudinal-transverse vibration such that the longitudinal component x_b and transverse component y_b act simultaneously and in phase. Mathematically this coupled motion can be treated as vibration applied along an axis that is at an arbitrary angle θ. The instantaneous displacement u of this sinusoidal vibrating motion along the axis of vibration is given by:

$$u = \begin{cases} u_a \sin\omega t & if\ t \ge t_v \\ 0 & if\ t < t_v \end{cases} \tag{23}$$

where u_a is the amplitude of the displacement of vibration and ω is the angular frequency in rad/s. The above equation acts as a switch that activates the sinusoidal vibration at $t \ge t_v$. The displacement components x_b and y_b in Fig. 3b are thus given by:

$$x_b = u\cos\theta \tag{24}$$
$$y_b = u\sin\theta \tag{25}$$

and the instantaneous velocity v of this sinusoidal motion along the axis of vibration is given by:

$$v = \begin{cases} u_a\omega\cos\omega t & if\ t \ge t_v \\ 0 & if\ t < t_v \end{cases} \tag{26}$$

where $u_a\omega$ is the amplitude of the velocity of vibration v_a, and hence:

$$v_a = u_a\omega = 2\pi f u_a \tag{27}$$

In longitudinal vibration, where θ is 0° or 180°, only x_b changes direction and y_b remains zero. In transverse vibration, where θ is 90° or 270°, only y_b changes direction and x_b remains zero. During any other mode of vibration, the vector direction of both x_b and y_b will change.

At the beginning of increment Δt the base touches the sliding body at point M. After the lapse of Δt, the base incremental displacements Δx_b and Δy_b (Fig. 4) are:

$$\Delta x_b = x_b - \boxed{x_b} \tag{28}$$

$$\Delta y_b = y_b - \boxed{y_b} \tag{29}$$

The effect of incremental displacement Δx_b is described by (14), whereas the effect of Δy_b by (30). Δy_b is only partially transferred to endpoint M [24], therefore, the displacement $\overline{M'^1 M_y'^2}$ of point M'^1 caused by the transverse component of vibrating motion comprises only a part of the incremental displacement Δy_b of the base:

$$\overline{M'^1 M_y'^2} = \eta_y \Delta y_b \tag{30}$$

where η_y is the transverse vibration transfer coefficient defining the proportion of Δy_b that is transferred to move the free endpoint from M'^1 to the M'^2 position. The consequence of this second phase of motion is a further change of asperity deformation from an intermediate s' to final magnitude s_1 (Fig. 4). Instantaneous direction of this deformation is determined by angle β, whilst the change in its magnitude by an increment $\Delta s'$ [24]. In similarity with the previous phase, $\Delta s'$ can be evaluated using relationship (6), therefore, the final magnitude of deformation s_1 after this second phase of motion is calculated by:

$$\begin{aligned} s_1 &= s' + \Delta s' \\ &= s' + v_{r2}\left[1 - \frac{k_t s'}{\mu F_N}\operatorname{sgn}(v_{r2})\right]^i \Delta t \end{aligned} \tag{31}$$

Relative velocity v_{r2} along the new line of action of the lumped elastic asperity can be determined from the following expression:

$$v_{r2} = \frac{\overline{N_1' M'^2} - \overline{N_1' M'^1}}{\Delta t} = \frac{\overline{N_1' M'^2} - s'}{\Delta t} \tag{32}$$

where

$$\begin{aligned} \overline{N_1' M'^2} &= \sqrt{[s'\cos\alpha]^2 + \left[s'\sin\alpha + \overline{M'^1 M_y'^2}\right]^2} \\ &= \sqrt{[s'\cos\alpha]^2 + \left[s'\sin\alpha + \eta_y \Delta y_b\right]^2} \end{aligned} \tag{33}$$

Direction of v_{r2} in relation to axis X is determined by angle β (Fig. 4) where:

$$\sin\beta = \begin{cases} \dfrac{s'\sin\alpha + \eta_y \Delta y_b}{\overline{N_1' M'^2}} & if\ t > t_v \\ 0 & if\ t \le t_v \end{cases} \tag{34}$$

$$\cos\beta = \begin{cases} \dfrac{s'\cos\alpha}{\overline{N_1' M'^2}} & if\ t > t_v \\ 1 & if\ t \le t_v \end{cases} \tag{35}$$

The if conditions in (34) and (35) are necessary to avoid nan errors in the formulation when $\overline{N_1'M'^2} = 0$. At the end of increment Δt, knowing the magnitude of deformation s_1 and its direction β, as well as coordinates $[x, y]$ of point N_1', it is possible to determine the coordinates of point M_1 at which the endpoint M is placed after lapse of increment Δt:

$$M_{1x} = N_{1x}' - s_1 \cos\beta \\ = x - s_1 \cos\beta \tag{36}$$

$$M_{1y} = N_{1y}' + s_1 \sin\beta \\ = y + s_1 \sin\beta \tag{37}$$

In accordance with relationship (1) and notations per Fig. 3 and Fig. 4, an instantaneous value of friction force components F_x and F_y can also be determined:

$$F_x(t + \Delta t) = k_t s_1 \cos\beta \tag{38}$$
$$F_y(t + \Delta t) = k_t s_1 \sin\beta \tag{39}$$

2.3. Consecutive time increments

The values of state variables listed in Table 1 computed during increment Δt are carried forward to the next consecutive time increment Δt_2. The sequence of equations (7) to (37) is then repeated to determine the coordinates of point M_2 at which the endpoint M is placed after lapse of time increment Δt_2. Equations (38) and (39) compute the components of friction force at the end of Δt_2. At consecutive increments ($3\Delta t$, $4\Delta t$,…, $n\Delta t$) the cycle described by these equations is repeated.

State variable	Computed during Δt by	Carried forward to Δt_2 for use as	
$\iint \frac{F_d - F_x}{m} dtdt$	(13)	$\boxed{\iint \frac{F_d - F_x}{m} dtdt}$	in (13)
x	(14)	$\boxed{x}$	in (8) and (14)
y	(16)	$\boxed{y}$	in (8)
x_b	(24)	$\boxed{x_b}$	in (28)
y_b	(25)	$\boxed{y_b}$	in (29)
Δx_b	(28)	$\boxed{\Delta x_b}$	in (14)
s_1	(31)	$\boxed{s_1}$	in (18) and (19)
M_{1x}	(36)	$\boxed{M_{1x}}$	in (7), (20) and (22)
M_{1y}	(37)	$\boxed{M_{1y}}$	in (7), (20) and (21)

Table 1: State variables

3. Methodology

The new model was evaluated by two methods; (i) in the Matlab®/Simulink® environment an analytical computation procedure was developed with equations (7) to (39) (ii) in Abaqus® the three-dimensional domain was numerically simulated by finite element method, with the model implemented via a specially developed friction subroutine defining the tangential contact behaviour between the body and base. The sliding body, Fig. 5, was a cuboid with contact area 0.030 m × 0.040 m and height 0.053 m, made up of deformable hexahedral elements. The base was a 0.1 m × 0.1 m analytical rigid shell. The material definition applied to deformable elements had Young's modulus 209 GPa and Poisson's ratio 0.3. There are two body masses m used in this paper; the density was set to 7850 kg/m^3 for a mass of 0.5 kg, or 31400 kg/m^3 for mass 2 kg. A spring element with stiffness k_d was applied between points A and B. A normal pressure load in addition to gravitational load was applied to attain a normal reaction

force F_N. The base orientation can be set between $0° \leq \theta < 360°$ in the XY plane, thereby applying any mode of in-plane vibration.

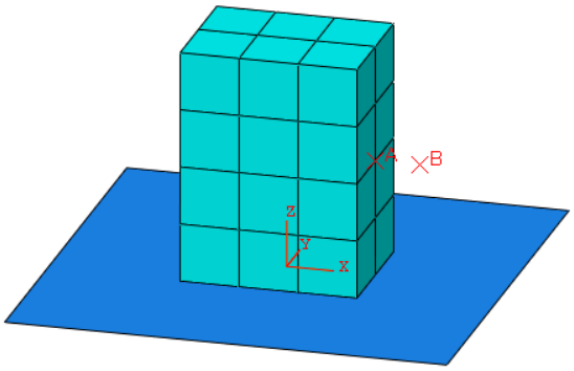

Fig. 5: 3D domain in Abaqus®

4. Results and discussion

In 4.1 and 4.2, results of longitudinal and transverse vibration are compared with analogous ones accepted in previous literature [23,24] that have shown a good match to experiments. Coupled longitudinal-transverse vibration is then evaluated in 4.3.

4.1. Longitudinal vibration

The longitudinal vibration model accepted in literature [23] was executed with the same parameters as utilised therein; $v_d = 0.0005$ m/s, $m = 0.5$ kg, $f = 4000$ Hz, $\mu = 0.1$, $F_N = 55$ N, $k_t = 80E6$ N/m. The value $k_d = 96068$ N/m was estimated by extracting data from graphs [23] and substituting into relationship (17). The total simulation time was set to 1 sec and a fixed time step of 1E-6 sec was utilised with vibration of the base starting at 0.14 sec. Fig. 6 illustrates the computed variability of drive force F_{dv} under the influence of longitudinal vibration in relation to the magnitude F_{ds} of this force without vibration as a function of a dimensionless coefficient $k_v = v_a/v_d$. Each data point on the graph corresponds to the result of a single simulation. The data points collectively form a trend indicated by the dashed line.

The new coupled vibration model proposed in this paper was then executed in Matlab®/Simulink® and Abaqus® using the same parameters while varying the value of k_v. To reduce computation effort in Abaqus® a larger time step of 1E-5 sec was utilised. The vibration mode was set to longitudinal by setting $\theta = 0°$. Since y_b given by (25) remains zero at $\theta = 0°$, $\overline{M'^1 M_y'^2}$ given by (30) also remains zero, therefore, the value of transverse vibration transfer coefficient η_y has no effect on the results of longitudinal vibration. Longitudinal vibration results obtained from the new model are also plotted in Fig. 6 and agree very well with the plotted trend. There is no reduction in drive force due to longitudinal vibration when $k_v \leq 1$.

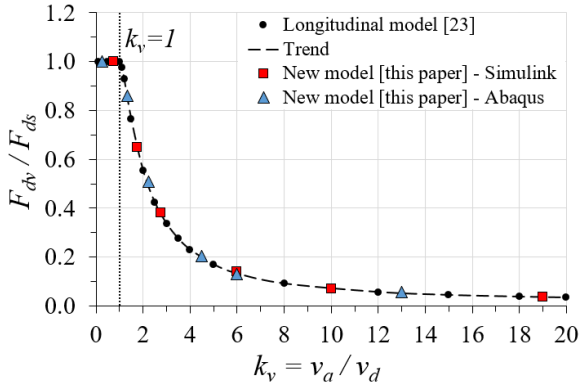

Fig. 6. Change in F_{dv}/F_{ds} as k_v increases in longitudinal vibration

Changes in drive force F_d and friction force F_x with time, computed using the new model when $k_v = 6$ ($v_a = 0.003$ m/s), are plotted in Fig. 7 and Fig. 8 in comparison to results obtained from the longitudinal vibration model [23]. Simulations begin with the body stationary, hence initially there is no elastic slip at the contact, resulting in $F_d = 0$ N at $t = 0$ sec (Fig. 7). Application of constant drive velocity v_d at $t > 0$ sec causes elastic deformation s to increase, resulting in a steady rise in F_d until $t \approx 0.12$ sec at which time breakaway occurs due to F_d reaching the magnitude of $\mu F_N = 5.5$ N. Switching on vibration at $t = 0.14$ sec significantly reduces the magnitude of F_d as the body continues to slide.

Also shown in Fig. 7, the new model when evaluated in Matlab®/Simulink® produces greater undulation of F_d. This is a characteristic of the new model and is due to the computation of x, equation (14), being different to how x is determined in the longitudinal model [23]. This undulation decreases as the vibration mode θ approaches transverse at 90° and 270°, see Fig. 10. F_{dv} is thus determined by averaging its magnitude within a single cycle:

$$F_{dv} = \frac{1}{n}\sum_{i=1}^{n} F_{dv_i}(t + \Delta t_i) \tag{40}$$

where n is the number of time intervals into which a single vibration cycle is divided:

$$n = \frac{1}{f\Delta t} \tag{41}$$

At $k_v = 6$ friction force component F_x undergoes cyclic changes in magnitude and direction (Fig. 8), therefore, its average value over a single vibration cycle reduces from $\mu F_N = 5.5$ N when there is no vibration to a lower value when vibration is initiated, hence the drive force is also reduced. Analytical results of the new model obtained via Matlab®/Simulink® show an exact match of F_x to the longitudinal model [23], however, numerical results from Abaqus® show subtle differences. These differences can be attributed to the Abaqus® solver which evaluates the model iteratively in each time increment to compute an approximation while enforcing equilibrium of internal structure forces with externally applied loads, whereas Matlab®/Simulink® performs an analytical calculation that outputs the exact solution to the formulation. These subtle differences in F_x affect the correlation of the Abaqus® computed drive force in Fig. 7, otherwise the new model agrees very well with previous work.

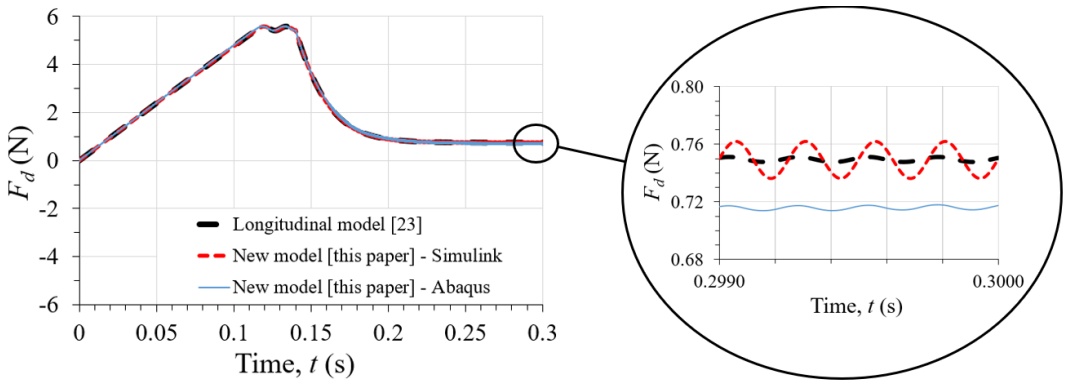

Fig. 7: Comparison of change in F_d when longitudinal vibration is switched on, $k_v = 6$

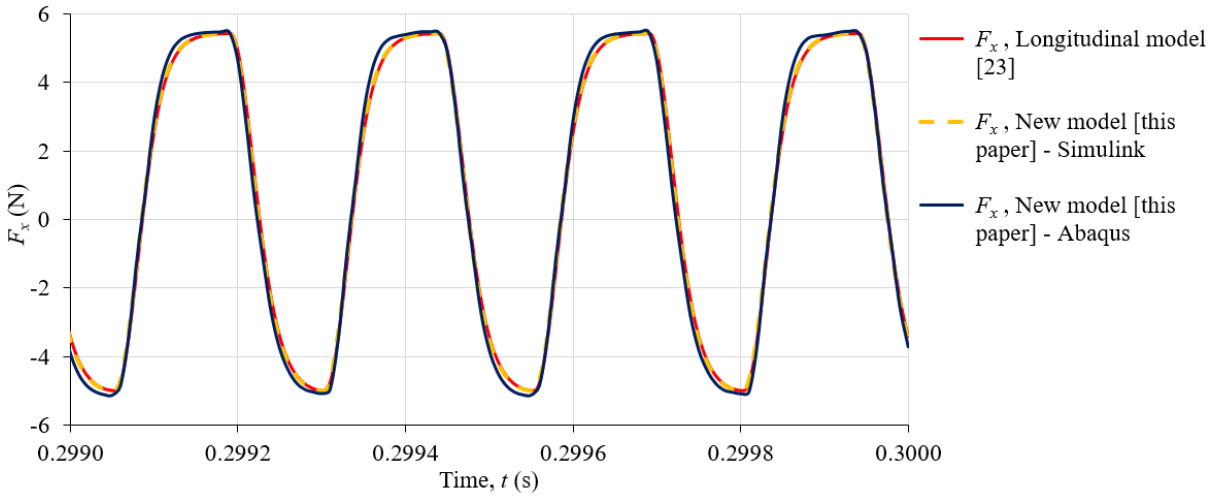

Fig. 8. *Comparison of friction force changes during longitudinal vibration, $k_v = 6$*

4.2. Transverse vibration

The new coupled model was executed for transverse vibration with parameters matching those utilised in literature [24]; $v_d = 0.0005$ m/s, $m = 2$ kg, $f = 3000$ Hz, $\mu = 0.1$, $F_N = 50.8$ N, $k_t = 67.29\text{E}6$ N/m, $k_d = 96068$ N/m. The total simulation time was set to 0.5 sec and a fixed time step of 1E-6 sec in Matlab®/Simulink®, and 1E-5 sec in Abaqus®, was utilised with vibration of the base starting at 0.14 sec. The vibration mode was set to transverse by setting $\theta = 270°$. The transverse vibration transfer coefficient was assumed $\eta_y = 0.71$. This is the value estimated by Gutowski and Leus [24] at which their transverse vibration model produces a good match to results of all experiments carried out at $f = 3000$ Hz in the range $v_d = 0.0001$-0.0033 m/s.

Fig. 9 illustrates the variability of normalised drive force F_{dv}/F_{ds} under the influence of transverse vibration as a function of a dimensionless coefficient k_v, computed using the transverse vibration model [24]. The data points, each corresponding to the result of a single simulation, form a trend indicated by the dashed line. Results obtained from the new model, overlaid in Fig. 9, agree very well with the trend. Unlike longitudinal vibration, in transverse vibration there is reduction of drive force even when $k_v \leq 1$.

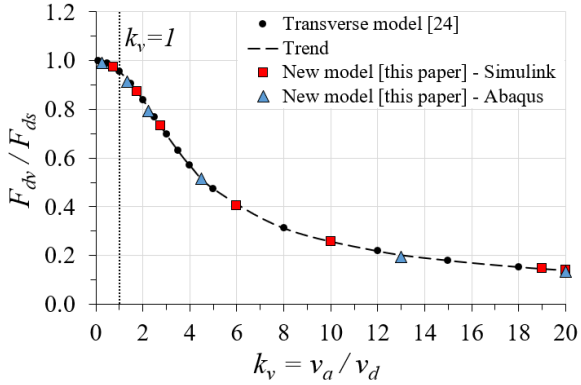

Fig. 9. Change in F_{dv}/F_{ds} as k_v increases in transverse vibration

Changes in drive force F_d, and friction force components F_x and F_y with time, computed using the new model when $k_v = 20$ ($v_a = 0.010$ m/s), are plotted in Fig. 10 and Fig. 11 in comparison to results obtained from the transverse vibration model [24]. Application of constant drive velocity v_d at $t > 0$ sec causes elastic deformation s to increase, resulting in a steady rise in F_d until $t \approx 0.11$ sec at which time breakaway occurs due to F_d reaching the magnitude of $\mu F_N = 5.08$ N. Switching on vibration at $t = 0.14$ sec significantly reduces the magnitude of F_d as the body continues to slide.

At $k_v = 20$, friction force component F_x undergoes cyclic changes only in magnitude whereas F_y changes in magnitude and direction, Fig. 11. The average value of F_x over a single vibration cycle reduces from $\mu F_N = 5.08$ N when there is no vibration to a lower value when vibration is initiated, hence the drive force is also reduced. Analytical results of the new model obtained via Matlab®/Simulink® show an exact match to the transverse model [24], and numerical results via Abaqus® show subtle differences attributed to the iterative solver.

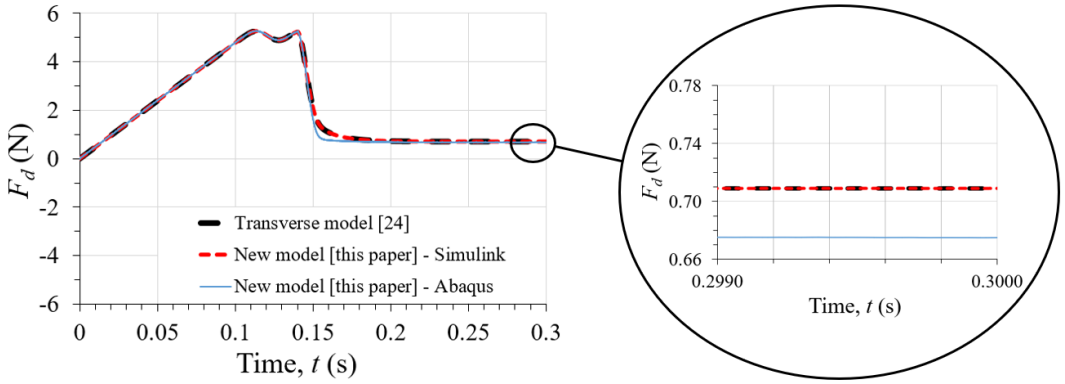

Fig. 10. Comparison of change in F_d when transverse vibration is switched on, $k_v = 20$

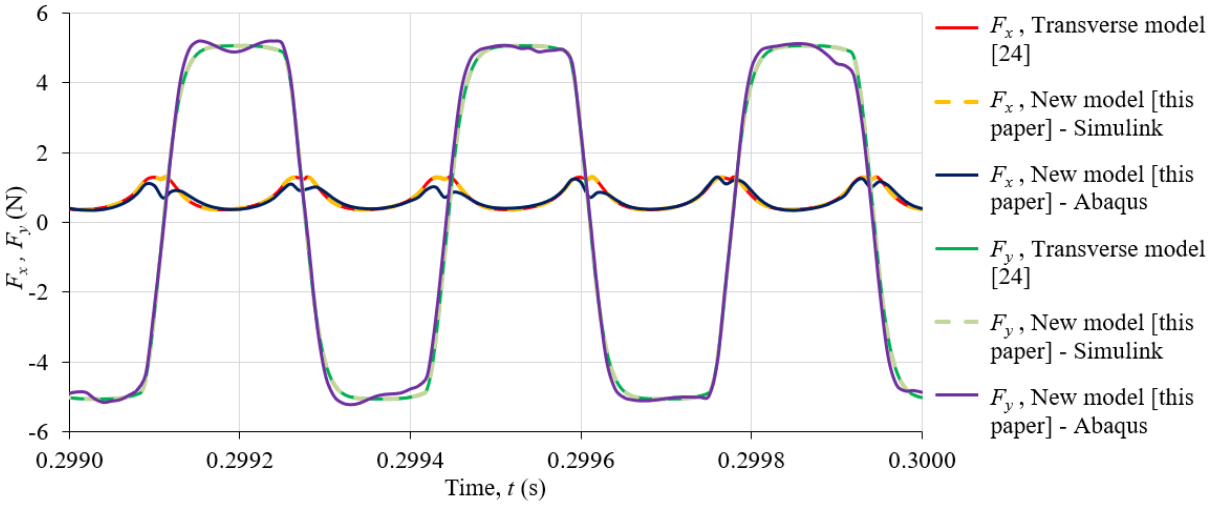

Fig. 11. Comparison of friction force changes during transverse vibration, $k_v = 20$

4.3. Coupled longitudinal-transverse vibration

The new model can also determine the influence of coupled longitudinal-transverse vibration on drive force F_d. Simulations were performed in different vibration modes θ at selected values of k_v (2, 3, 4, 6 and 20) with parameters described in 4.2; $v_d = 0.0005$ m/s, $m = 2$ kg, $f = 3000$ Hz, $\mu = 0.1$, $F_N = 50.8$ N, $k_t = 67.29$E6 N/m, $k_d = 96068$ N/m. The total simulation time was set to 0.5 sec and a fixed time step of 1E-6 sec in Matlab®/Simulink®, and 1E-5 sec in Abaqus®, was utilised with vibration of the base starting at 0.14 sec. At $\eta_y = 0.71$ the transverse vibration model [24] produces a good match to results of all transverse vibration experiments performed at $f = 3000$ Hz in the range $v_d = 0.0001$-0.0033 m/s. Since the vibration frequency in the transverse direction will remain 3000 Hz at all vibration modes θ, and v_d is also in the range 0.0001-0.0033 m/s, it is reasonable to assume $\eta_y = 0.71$ for all vibration modes.

For each selected value of k_v simulations in 25 different vibration modes θ were performed in Matlab®/Simulink®. The results in terms of normalised drive force F_{dv}/F_{ds} are plotted in Fig. 12 and the corresponding trend for each value of k_v is also plotted. 3 further simulations for each value of k_v were performed in Abaqus® and their results are also overlaid in Fig. 12. Abaqus® and Matlab®/Simulink® results are in good agreement; an increase in k_v results in a decrease in the drive

force in all modes of vibration. Regardless of the value of k_v the greatest reduction in drive force is always achieved by longitudinal vibration ($\theta = 0°, 180°$). During transition from longitudinal to transverse vibration ($\theta = 90°, 270°$), and vice versa, the shape of curve F_{dv}/F_{ds} varies depending on the value of k_v, however, the curve is always symmetrical about $\theta = 180°$. This suggests the same result can be obtained at multiple values of θ.

5. Substituting Dahl with LuGre friction model

The new model is based on friction behaviour per the Dahl model [31], however, it is possible to substitute other dynamic friction models into the formulation, for example, the LuGre friction model [32] which is an extension of the Dahl model and defines the friction force by extending relationship (1) to:

$$F = k_t s + h_t \frac{ds}{dt} + h_v v_r \tag{42}$$

where h_t is the contact damping coefficient, h_v is the viscous damping coefficient, and ds/dt is given by:

$$\frac{ds}{dt} = v_r - \frac{k_t|v_r|}{\mu F_N + (F_S - \mu F_N)e^{-(v_r/v_s)}} s \tag{43}$$

where F_S is the stiction force and v_s is the Stribeck velocity. Equations (18) and (31) are then substituted by (44) and (45):

$$s' = \boxed{s_1} + \left[v_{r1} - \frac{k_t|v_{r1}|}{\mu F_N + (F_S - \mu F_N)e^{-(v_{r1}/v_s)}} \boxed{s_1} \right] \Delta t \tag{44}$$

$$s_1 = s' + \left[v_{r2} - \frac{k_t|v_{r2}|}{\mu F_N + (F_S - \mu F_N)e^{-(v_{r2}/v_s)}} s' \right] \Delta t \tag{45}$$

and, (38) and (39) substituted by (46) and (47):

$$F_x(t + \Delta t) = \left[k_t s_1 + h_t \left(\frac{s_1 - \boxed{s_1}}{dt} \right) + h_v \left(\frac{\overline{N_1' M'^2} - \boxed{s_1}}{\Delta t} \right) \right] \cos\beta \tag{46}$$

$$F_y(t + \Delta t) = \left[k_t s_1 + h_t \left(\frac{s_1 - \boxed{s_1}}{dt} \right) + h_v \left(\frac{\overline{N_1' M'^2} - \boxed{s_1}}{\Delta t} \right) \right] \sin\beta \tag{47}$$

Setting $h_t = h_v = F_S = 0$ in the LuGre model reverts to Dahl friction behaviour. To prove this the LuGre model was implemented into the new coupled vibration model for execution in Matlab®/Simulink® at $k_v = 2$ and 20. Results using the LuGre model are overlaid in Fig. 12 and show an exact match to those with Dahl friction.

If h_t, h_v, and F_S are non-zero, or if another friction model is used then the value of the transverse vibration transfer coefficient η_y may change since $\eta_y = 0.71$ is based on a fit fidelity exercise performed by Gutowski and Leus [24] to match their model, which is also based on Dahl friction, to experimental data. If the friction model is changed it is advisable to check the fit fidelity of the model to experimental results and use a new value of η_y if necessary.

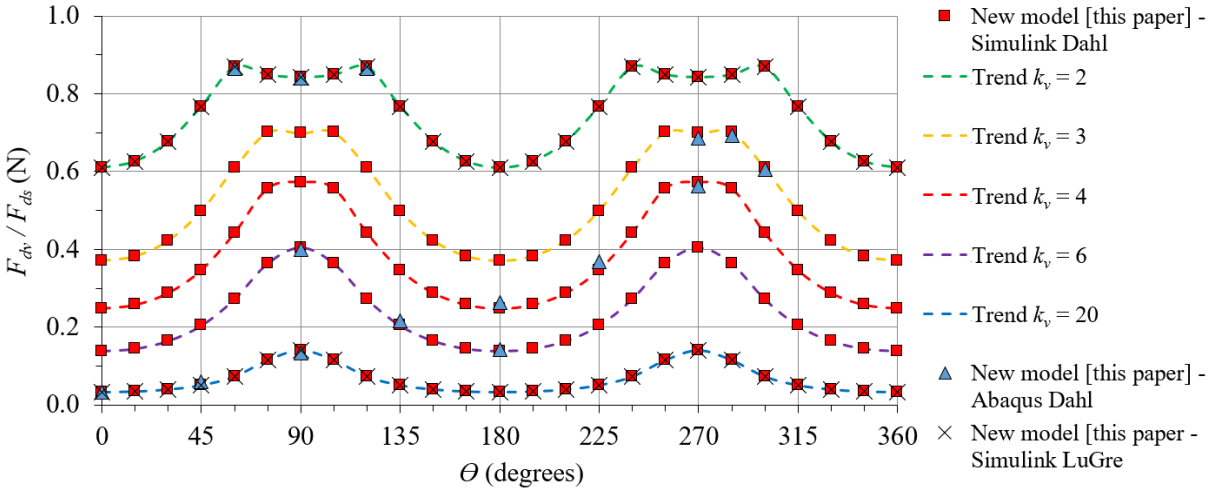

Fig. 12. Changes in F_{dv}/F_{ds} with θ at different values of k_v

6. Conclusion

A new analytical model has been developed based on two separate models presented in previous literature [23,24]. The new model is able to describe changes in friction force and drive force during sliding motion of a body over a surface vibrating not only in the longitudinal or transverse mode but also in any mode of coupled longitudinal-transverse vibration. The model has been evaluated analytically in Matlab®/Simulink® and numerically via a specially developed friction subroutine in Abaqus®. Simulations yield good agreement with the models for longitudinal [23] and transverse vibration [24] in previous literature.

The new model can be used in any three-dimensional domain, such as the flat-on-flat contact domain used in this paper where the normal contact pressure has been assumed constant, or a more complex case of gears for example, where the normal contact pressures change as gear teeth move over one another, while multiple teeth enter and exit the gear mesh forming multiple contacts simultaneously. An advantage with Abaqus® is that the complexity of the domain can be increased by modifying the geometry of parts within it and the way in which they interact, whereas in Matlab®/Simulink® additional relationships would have to be introduced to describe these aspects which may result in time-varying contact geometry. In the case of flat-on-flat contact, the greatest reduction in F_d is achieved by longitudinal vibration, however, friction is in nearly all engineering problems and in other applications a different vibration mode may be more beneficial.

To simulate coupled vibration the value of transverse vibration transfer coefficient η_y must be known and can be estimated using transverse vibration experimental data with the method described by Gutowski and Leus [24]. It is assumed that η_y does not change in value as vibration mode θ changes. The new model can then be used to compute changes in friction force and drive force in any mode of vibration. The longitudinal model and transverse model have previously been validated against experiments [23,24] and have been used in this paper as basis for validating the new model, however, experimental results for coupled vibration are not currently available. This provides scope for future work. Also, the influence on η_y of using dynamic friction models other than the Dahl model is currently unknown.

References

[1] Hargreaves DJ, Planitz A. Assessing the energy efficiency of gear oils via the FZG test machine. Tribology International 2009;42(6):918-25.

[2] Marques PMT, Fernandes CMCG, Martins RC, Seabra JHO. Efficiency of a gearbox lubricated with wind turbine gear oils. Tribology International 2013;71:7-16.

[3] Cardoso NFR, Martins RC, Seabra JHO, Igartua A, Rodríguez JC, Luther R. Micropitting performance of nitrided steel gears lubricated with mineral and ester oils. Tribology International 2009;42(1):77-87.

[4] Shen M, Luo J, Wen S. The tribological properties of oils added with diamond nano-particles. Tribology Transactions 2001;44(3):494-8.
[5] Chu HY, Hsu WC, Lin JF. The anti-scuffing performance of diamond nano-particles as an oil additive. Wear 2010;268(7):960-7.
[6] Zhou G, Zhu Y, Wang X, Xia M, Zhang Y, Ding H. Sliding tribological properties of 0.45% carbon steel lubricated with Fe3O4 magnetic nano-particle additives in base oil. Wear 2013;301(1-2):753-7.
[7] Moorthy V, Shaw BA. Contact fatigue performance of helical gears with surface coatings. Wear 2012;276-277:130-40.
[8] Xiao Y, Shi W, Luo J, Liao Y. The tribological performance of TiN, WC/C and DLC coatings measured by the four-ball test. Ceramics International 2013;40(5):6919-25.
[9] Baker HD, Claypoole W, Fuller DD. Proceedings of the First US National Congress of Applied Mechanics 1952;23.
[10] Fridman HD, Levesque P. Reduction of static friction by sonic vibrations. Journal of Applied Physics 1959;30(10):1572-5.
[11] Godfrey D. Vibration reduces metal to metal contact and causes an apparent reduction in friction. Tribology Transactions 1967;10(2):183-92.
[12] Lenkiewicz W. The sliding friction process-effect of external vibrations. Wear 1969;13(2):99-108.
[13] Hess DP, Soom A. Normal vibration and friction under harmonic loads: Part I-Hertzian contacts. Journal of Tribology 1991;113(1):80-6.
[14] Abdo J, Tahat M. The Effect of Frequency and Amplitude of Vibration on the Coefficient of Friction for Metals. WSEAS Transactions on Applied and Theoretical Mechanics 2008;3(7):265-74.
[15] Chowdhury MA, Helali MM. The effect of amplitude of vibration on the coefficient of friction for different materials. Tribology International 2008;41(4):307-14.
[16] Mitskevich AM. Motion of the body over tangentially vibrating surface taking account of friction. Soviet Physics-Acoustics 1968;13(3):343-51.
[17] Skare T, Stahl JE. Static and dynamic friction processes under the influence of external vibrations. Wear 1992;154(1):177-92.
[18] Mutuonga S, Onoda J. New gravity compensation method by dither for low-g simulation. Journal of Spacecraft and Rockets 1995;32(2):364-9.
[19] Littmann W, Storck H, Wallaschek J. Sliding friction in the presence of ultrasonic oscillations: superposition of longitudinal oscillations. Archive of Applied Mechanics 2001;71(8):549-54.
[20] Littmann W, Storck H, Wallaschek J. Reduction of friction using piezoelectrically excited ultrasonic vibrations. Proceedings of SPIE - The International Society for Optical Engineering 2001;4331:302-11.
[21] Storck H, Littmann W, Wallaschek J, Mracek M. The effect of friction reduction in presence of ultrasonic vibrations and its relevance to travelling wave ultrasonic motors. Ultrasonics 2002;40(1-8):379-83.
[22] Kumar VC, Hutchings IM. Reduction of sliding friction of metals by the application of longitudinal or transverse ultrasonic vibration. Tribology International 2004;37(10):833-40.
[23] Gutowski P, Leus M. The effect of longitudinal tangential vibrations on friction and driving forces in sliding motion. Tribology International 2012;55(6):108-18.
[24] Gutowski P, Leus M. Computational model for friction force estimation in sliding motion at transverse tangential vibrations of elastic contact support. Tribology International 2015;90:455-62.
[25] Tsai CC, Tseng CH. The effect of friction reduction in the presence of in-plane vibrations. Archive of Applied Mechanics 2006;75(2):164-76.
[26] Jimma T, Kasuga Y, Iwaki N, Miyazawa O, Mori E, Ito K, Hatano H. An application of ultrasonic vibration to the deep drawing process. Journal of Materials Processing Technology 1998;80-81:406-12.
[27] Siegert K, Ulmer J. Influencing the Friction in Metal Forming Processes by Superimposing Ultrasonic Waves. CIRP Annals - Manufacturing Technology 2001;50(1):195-200.

[28] Egashira K, Mizutani K, Nagoa T. Ultrasonic Vibration Drilling of Microholes in Glass. CIRP Annals - Manufacturing Technology 2002;51(1):339-42.
[29] Schneider Y, Zahn S, Schindler C, Rohm H. Ultrasonic excitation affects friction interactions between food materials and cutting tools. Ultrasonics 2009;49(6-7):588-93.
[30] Dahl P. A Solid Friction Model. Technical Report TOR-0158H3107-181-1. The Aerospace Corporation, El Segundo, CA 1968.
[31] Dahl P. Solid friction damping of mechanical vibrations. AIAA Journal 1976;14(12):1675-82.
[32] Canudas de Wit C, Olsson H, Astrom KJ, Lischinsky P. A new model for control of systems with friction. IEEE Transactions on Automatic Control 1995;40(3):419-25.